Material Survivability on Launch of Slender Ballistic Range Projectiles

A. R. Dworzanczyk* N. J. Parziale[†]
Stevens Institute of Technology, Hoboken, NJ 07030, USA
N. J. Mueschke [‡]   D. J. Grosch[§]   P. Bueno[¶]
Southwest Research Institute, San Antonio, TX, 78238, USA

To study particulate and precipitation effects on high-speed vehicles, slender projectiles were fabricated from different relevant materials and subjected to ballistic range experiments. The materials were selected for their applicability to future aerospace structures and include 625 Inconel, 2-D carbon-carbon composite, and fully-dense alumina. The ballistic range tests were carried out at Southwest Research Institute's (SwRI) Light Gas Gun (LGG) facility to determine material suitability for future studies of the interaction of high-speed projectiles with multiphase flow fields, and required subjecting the projectiles to accelerations in excess of 70,000 G. Only the 625 Inconel projectiles survived launch during the experiment. Projectiles fabricated from 2-D carbon-carbon and from alumina shattered during launch. Schlieren, X-ray, and high-speed optical images of each projectile were collected to study the manner of flight and/or breakup of each projectile. In order to avoid failure in the future, the projectiles were totally redesigned into blunt-nosed, full-bore-rider projectiles. The new designs were analyzed using finite element analysis to increase confidence that they will survive launch during a new round of tests.

I. Nomenclature

σ_c = compressive yield stress of material
σ_t = tensile yield stress of material
$\sigma_{1,2,3}$ = principal stresses in material

II. Introduction

Particulates and precipitation can have numerous deleterious effects on high-speed vehicles [1]. Impacts with droplets or small particles at high velocity can degrade aerospace materials, reducing transparency and other desirable properties [2]. The small length scales involved in multiphase interactions with precipitation and suspended particulates mean that the bulk mechanical properties of a material are not always useful for estimating the effects of these interactions. The granular properties of a material can greatly impact whether the material fails in multiphase, hypersonic flow applications [3, 4]. At the same time, the interaction of the shock structure around a vehicle can disrupt a droplet, potentially altering the deleterious effects of impact [5–7]. At speeds less than 4 km/s, droplets are known to break up in high-speed air flows primarily through an edge-stripping model. That is, droplets flatten out and lose mass as smaller droplets are shed from their circumference. At very high Mach numbers, droplets have been observed to catastrophically disintegrate due to surface instability [5]. Since the sphericity and mass of an impacting drop both impact the degree of damage it does to relevant materials in a high-speed collision [3], it is important to characterize the exact breakup behavior of droplets in a multiphase flow system around an aerospace structure. Our approach is to use the Southwest Research Institute (SwRI) Light Gas Gun (LGG) facility to accelerate relevant materials to high velocities, introduce some prescribed form of precipitation, and study the multiphase flow interactions using advanced diagnostic techniques [8, 9]. In this paper, we describe an original slender design, some preliminary results where the slender design was found to be insufficiently strong, and then we present redesigned projectiles in an attempt to eliminate the design flaws.

Material	625 Inconel[11, 12]	Fully-Dense Alumina[13]	2D Carbon-Carbon[14]
Density (kg/m^3)	8581	3900	1700
Modulus of Elasticity (Pa)	1.93E8	3.5E11	5.00E10
Thermal Conductivity (W/(m K))	9.8	28	26
Heat Capacity (J/(kg K))	410	880	720
Coefficient of Thermal Expansion (K^{-1})	1.28E-5	8.40E-6	1.00E-5
Tensile Yield Strength (Pa)	4.14E8	2.60E8	1.20E8

Table 1   Table 1: Projectile Material Properties

III. Initial Projectile Design and Fabrication

The LGG facility is a multistage gas gun capable of accelerating projectiles to over 2,500 m/s [10]. It is depicted in Fig. 1. The acceleration required to reach this velocity is up to 7E5 m/s/s, or approximately 71,000 G.

Fig. 1   Southwest Research Institute Light Gas Gun

Three materials were chosen for testing in the LGG. The first of these, 625 Inconel, is a nickel alloy with a long history of use in aerospace applications requiring consistent mechanical properties at extreme temperatures. The second, fully-dense alumina, is of interest for radome and other sensor cover applications because of its transparency in the infrared spectrum. The final material, 2D carbon-carbon composite, is of interest for its light weight and high strength-to-weight ratio. Density and other mechanical properties of these materials are tabulated in Tab. 2.

The projectiles were manufactured to a shape dictated by the limits of vendor machine-tool precision and the size of the sabot in which the projectile had to be enclosed during launch. Each projectile is a cone with a half-angle of 5 degrees. The cone is, in each case, 1" wide at its maximum diameter. The projectile is 5.581" long, with a 1/32" tip radius. The Inconel and alumina cones were hollowed out in an effort to improve aerodynamic stability by moving the center of mass forward. For these projectiles, a small aluminum frustum, with major and minor diameters of 0.817" and 0.500" and a length of 0.158", was placed in the projectile base to distribute launch loads onto the sabot. Both hollow and solid carbon-carbon projectiles were manufactured, but a solid (that is, not hollow) carbon-carbon projectile was launched in the hope that it would be more likely to survive launch stresses. A technical drawing of the hollow and solid projectiles is given in Fig. 2. An image of the alumina projectile, with its frustum and sabot, is given in Fig. 3.
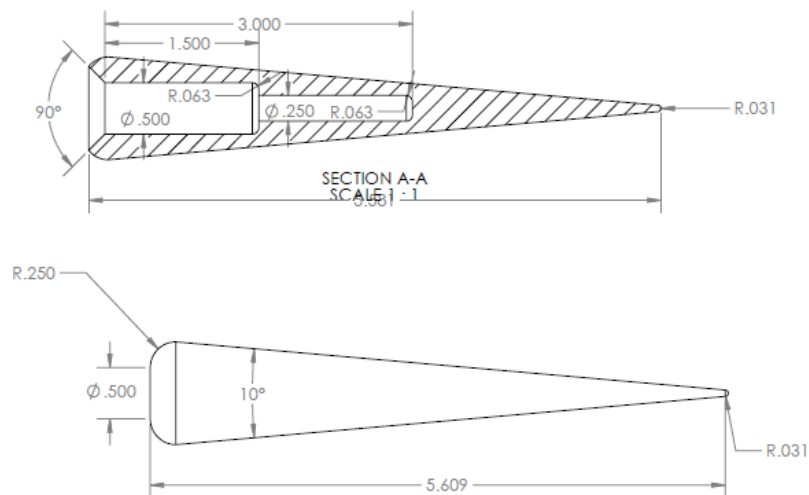
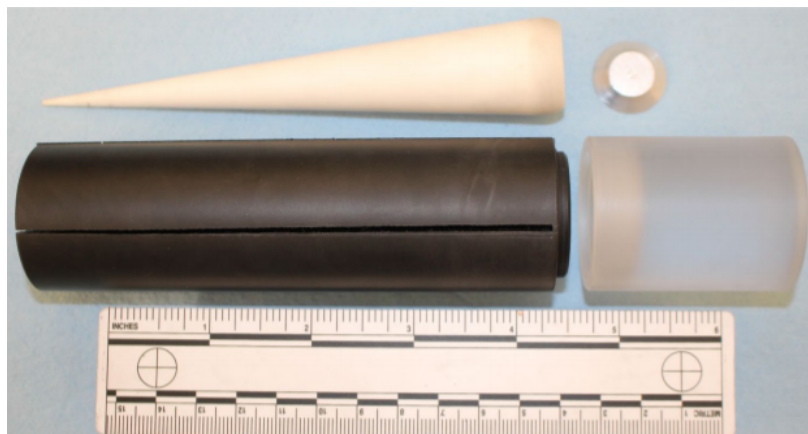**Fig. 2   Hollow and Solid Projectile Schematic**

Fig. 3   Hollow Alumina Projectile with Frustum, Sabot, and ruler for scale

IV. Test Shots and Results

Four shots were carried out during the week of March 15, 2021 at the LGG facility. The first shot, using 625 Inconel, resulted in a damage to the projectile before it could be imaged. The sabot did not cleanly separate from the projectile and interfered with its flight, resulting in a collision that caused a noticeable bend in the projectile. A Schlieren image collected during this test illustrates the bend in Fig. 4.

The second shot also used a projectile made from 625 Inconel. During this shot, the sabot separated cleanly from the projectile, which passed into the schlieren imaging field without damage. Images were collected. With advanced lasers and cameras, the authors hope the schlieren image quality can be improved. A schlieren image from this test is given in Fig. 5.

The third shot was carried out with a hollow fully-dense alumina projectile. This shot resulted in projectile breakup. The article failed under launch loads and shattered during sabot separation. X-ray images collected during the shot reveal crack propagation from several different locations in the projectile, including at a region where the internal hollow volume comes particularly close to the outer surface. X-ray and visible light images of the fractured projectile are given in Fig. 6 and Fig. 7.

The final shot carried out used a solid 2D carbon-carbon composite projectile. Because this projectile was solid, no
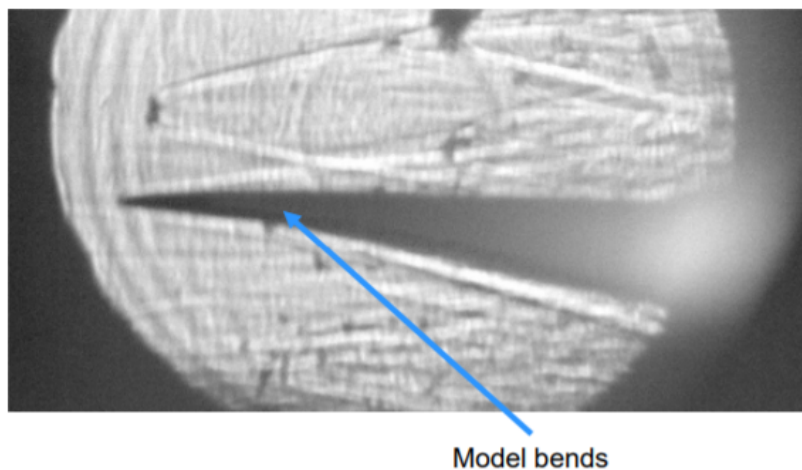
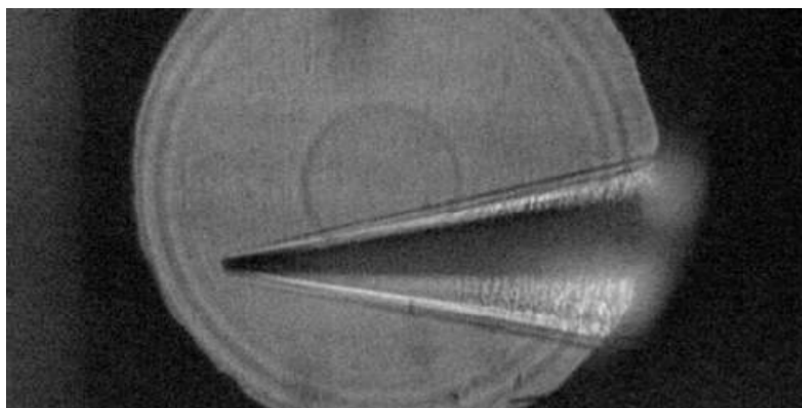**Fig. 4   Schlieren Image of Inconel Shot with Damaged Projectile**

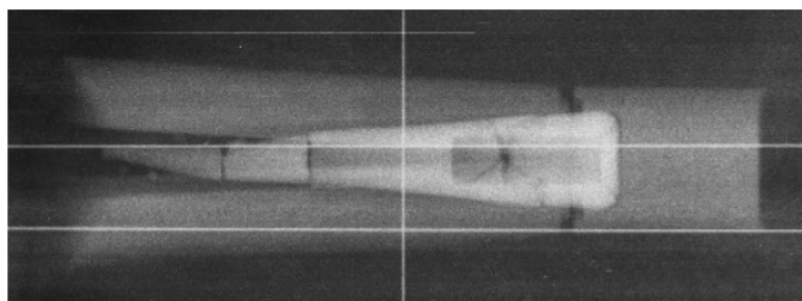**Fig. 5   Schlieren Image of Inconel Shot without damage**

Fig. 6   X-ray image of Alumina projectile showing largest cracks

aluminum frustum was included in this shot. This projectile splintered and disintegrated during launch. Because of the greater transparency of carbon-carbon composite than alumina in the X-ray spectrum, no obvious center of crack propagation can be seen in the X-ray images collected during this test shown in Fig. 8. Visible-light images in Fig. 9 show a breakup into at least three large chunks and a large number of much smaller fragments. Two of these large chunks can be seen in Schlieren images, as shown in Fig. 10.

While long, tapered projectiles fabricated from Inconel 625 survived launch, projectiles fabricated from more brittle materials like fully-dense alumina did not. X-ray and visible light images indicate that the points of failure for the
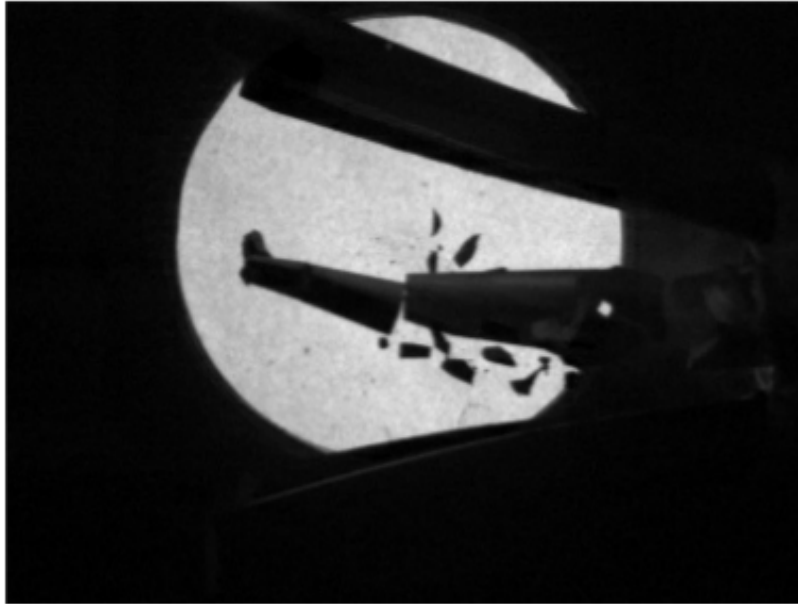
4

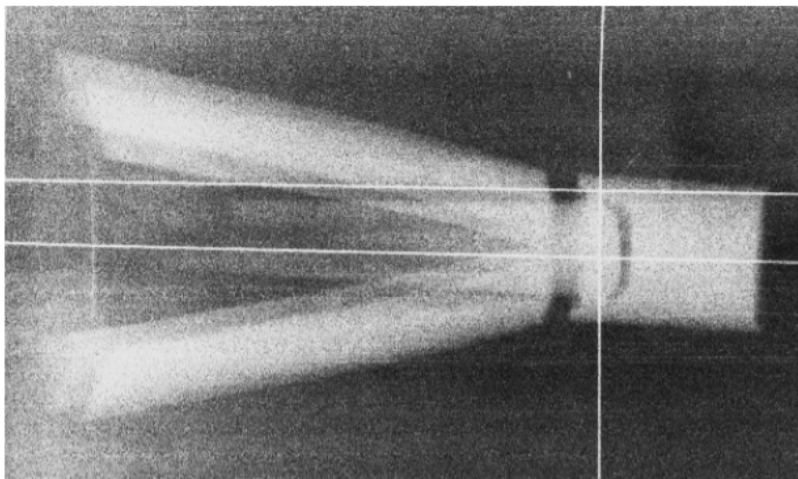**Fig. 7   Visible light image of fractured alumina projectile in flight**

Fig. 8   X-ray image of Carbon-Carbon Projectile in flight

alumina projectiles were located near regions of predicted stress concentrations. The pointed tip in particular, and regions where the alumina projectile had been hollowed out to move the center of mass forward, were vulnerable. It is hypothesized that stress waves during launch propagated through the structure and became focused at the tip of the slender projectile body.

Furthermore, the use of sabots on these projectiles caused issues with incomplete sabot separation. Fig. 11 shows the results of a sabot impacting the striker plate too close to the pass-through. If the sabot does not separate cleanly from the projectile, it can interfere with the projectile's flight, and ruin an otherwise-successful shot.

V. Projectile Redesign

During 2021, the projectile design was altered in an effort to improve test reliability. A full-bore-rider design was used instead of a discarding sabot to eliminate sabot separation and fit concerns. In the new design, a polycarbonate base of diameter 1.535" completely fills the bore of the light-gas gun and is secured to a tip made from an material

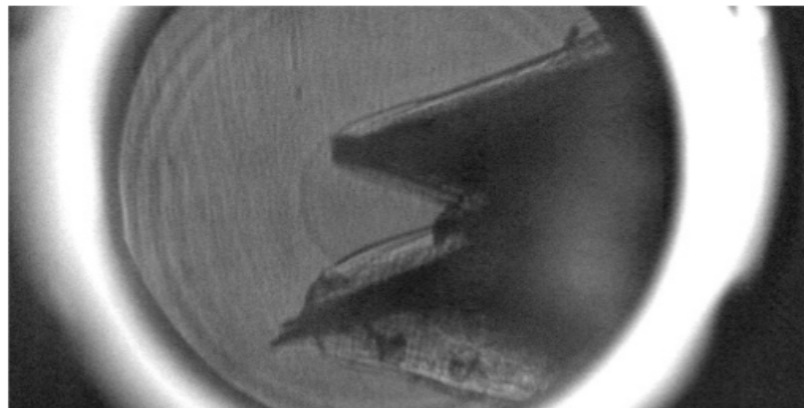**Fig. 9   Visible light image of fractured carbon-carbon projectile in flight**

Fig. 10   Schlieren image of fractured carbon-carbon projectile in flight

of interest. This tip is made of an aerospace material of interest (like fully-dense alumina) adhered with epoxy to a metal holder. This metal holder screws into the polycarbonate projectile base. The aerospace material tip thus avoids threads and other stress concentrations, improving survivability. A 75%/25% tungsten-copper alloy (10W3) was chosen as a compromise for high density and ease of machining. In a previous hypersonic projectile test by Bogdanoff and Wilder [15], a Tracon epoxy was used to adhere the projectile tip to the main body. Because of supply chain issues that made this epoxy unavailable, a similar compound, Loctite Ablestik 2112, was substituted.

To further reduce stress concentrations on the projectile tip, it is redesigned from a slender cone to a spherical dome with a mostly-flat aft face. The aft face is secured by epoxy to the cup-shaped tip holder. It is believed that redesigning the projectile tip to a spherical dome will eliminate the stress concentrations that doomed the slender alumina and carbon-carbon projectiles.

A schematic of the assembled projectile is depicted in Fig. 12

VI. Projectile Finite Element Analysis

To increase confidence that the revised projectile design would survive the expected launch stresses in the SwRI LGG facility, an explicit dynamics simulation was carried out in ANSYS. The expected acceleration vs. time curve was converted into an applied pressure vs. time curve by multiplying acceleration by the 0.25 kg projectile mass and dividing by cross-sectional area. Appropriate contact conditions were selected for the epoxy and thread surfaces. The

6

Fig. 11   Impact of Sabot hitting striker plate too close to pass-through
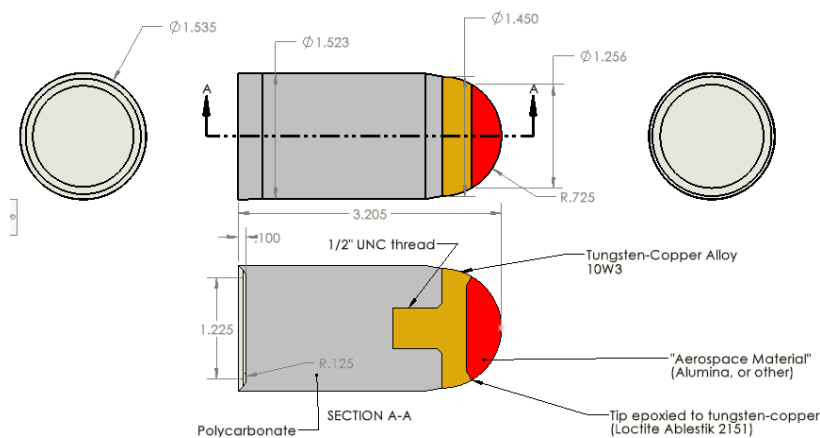

Fig. 12   Assembled Projectile Schematic with Center of Mass Marked

stress distributions in the three parts of the projectile were analyzed when the average acceleration of the projectile assembly exceeded the maximum expected value. Material properties were specified according to Table 2.

Southwest Research Institute supplied three acceleration vs. time curves for 0.25 kg projectiles. The acceleration curves for 0.25 kg projectiles supplied by Southwest Research Institute is supplied in Fig. 13. The 1D hydrocode prediction for gun performance overpredicts gun muzzle velocity for a given propellant load by about 10%. To compensate for this tendency, SwRI includes a knockdown factor of 10% to 12%–that is, the code optimizes the propellant load for a muzzle velocity 88% to 90% as great as the desired velocity. The acceleration profile calculated for a 12% knockdown factor, therefore, represents the most aggressive launch profile, and this profile is the one used in the explicit dynamics simulations carried out in support of the projectile redesign effort. The acceleration profile is converted into a time-varying pressure boundary condition on the aft face of the full bore rider projectile in the ANSYS explicit dynamics simulation by multiplying the acceleration by the projectile mass and dividing by the cross-sectional area. A 0 radial displacement boundary condition is applied to the outer surface of the polycarbonate projectile base because, in practice, the steel gun barrel would prevent radial deformation. Fig. 14 illustrates the applied boundary conditions for the explicit dynamics simulation.

7

Material	Tungsten-Copper 10W3 [16]	Fully-Dense Alumina[13]	Polycarbonate Plastic[17]
Density (kg/m^3)	14900	3900	1200
Modulus of Elasticity (Pa)	2.6E11	3.5E11	2.2E9
Coefficient of Thermal Expansion (K^{-1})	8.5E-6	8.40E-6	7.02E-5
Tensile Yield Strength (Pa)	5.85E8	2.6E8	7.2E7
Poisson's Ratio	0.2875	0.22	0.3182
Bulk Modulus (Pa)	2.04E11	2.20E11	1.93E9
Shear Modulus (Pa)	1.01E11	1.52E11	7.97E8

Table 2   Table 2: Redesigned Projectile Material Properties used in ANSYS Explicit Dynamics Simulation

The chosen acceleration profile shows a maximum expected acceleration of almost 7E5 m/s^2. When the average acceleration of the simulated projectile reaches or exceeds this value, the simulation is stopped and stresses on the projectile components are reported. Since the acceleration at the step at which stresses are reported will actually exceed 7E5 m/s^2, by approximately 20%, the reported stress values calculated by ANSYS are considered conservative.
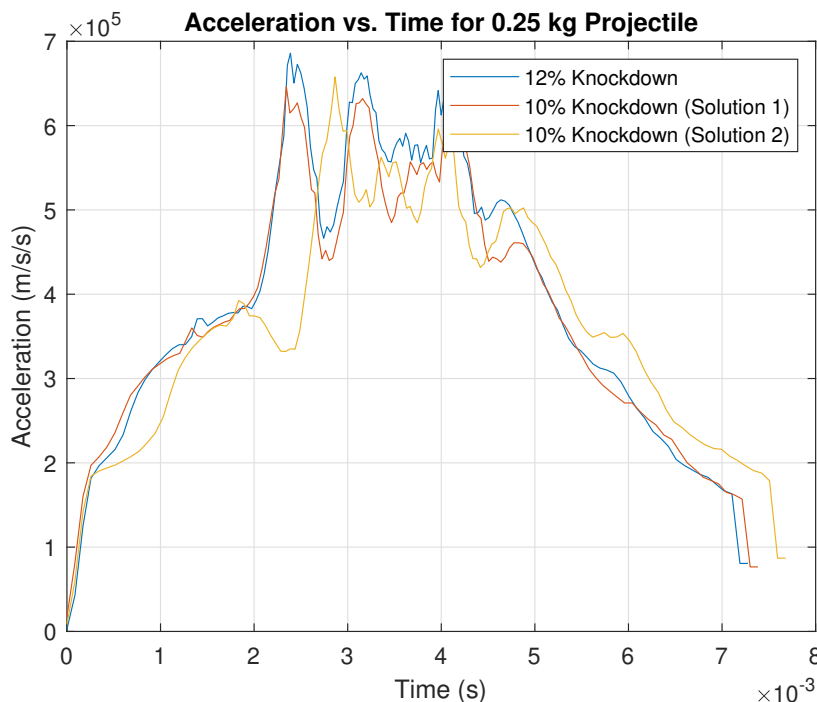

Fig. 13   Acceleration vs. Time Curves supplied by SwRI

The simulated projectile tip and tip holder are meshed with an unstructured grid with a body sizing of 2 mm. The polycarbonate base also uses an unstructured grid with 2 mm body sizing, except near where the tungsten-copper projectile holder contacts it. In this region, a mapped mesh with a 0.5 mm edge sizing is used. The total number of elements is 188,525, and the mesh is depicted in Fig. 15.

Fig. 16 gives the stress distribution on the flat, aft face of the fully-dense alumina projectile tip at peak acceleration. The compressive stress here reaches a maximum value of 165 MPa. This is far below (by a safety factor of 14) the yield stress of fully dense alumina in compression (2.6 GPa). The maximum stress is reached in an annular region on the aft face of the tip. No stress concentration was observed in the simulation results. Fig. 17 shows the safety factor distribution for this component.
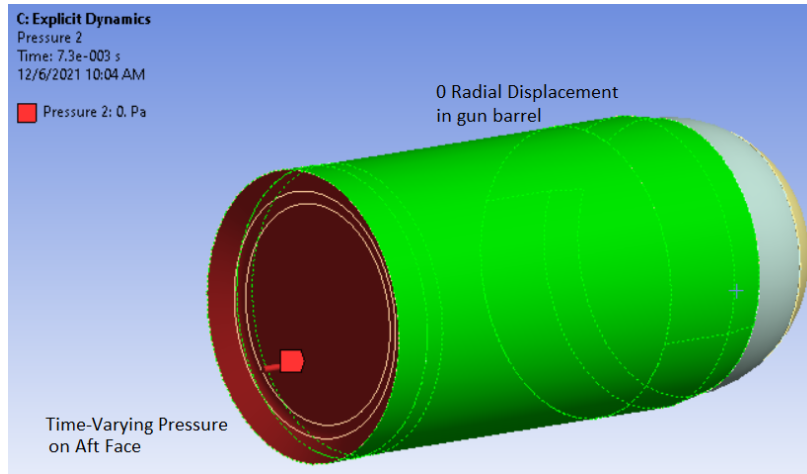
8

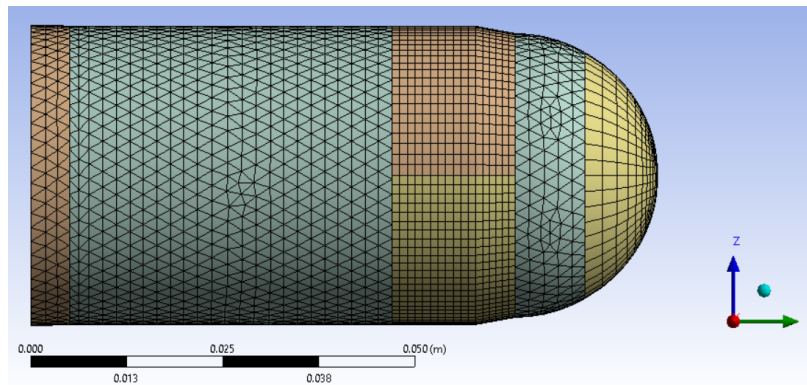**Fig. 14   Simulation Boundary Conditions**

Fig. 15   Mesh used in Projectile Explicit Dynamics Simulation

Fig. 18 gives the stress distribution in a section view along the middle of the tungsten-copper projectile tip holder. The maximum stress in the this component is 464 MPa. This stress is reached in the filleted region immediately forward of the holder's threads. This is an expected stress concentration location. The yield stress of the tungsten-copper alloy is 585 MPa, so a safety factor of 1.26 is maintained even in this conservative analysis. Fig. 19 shows the safety factor distribution in the tungsten-copper tip holder.

The maximum principle stresses in the alumina tip were also compared to the Christensen failure criterion for fully-dense alumina. The Christensen failure criterion [18] relates the principle stresses in an isotropic material to the material's tensile and compressive yield stresses:

$$(\frac{1}{\sigma_t} - \frac{1}{\sigma_c})(\sigma_{xx} + \sigma yy + \sigma zz) + \frac{1}{\sigma_t \sigma_c}\{\frac{1}{2}[(\sigma_{xx} - \sigma_{yy})^2 + (\sigma_{yy} - \sigma_{zz})^2 + (\sigma_{zz} - \sigma_{xx})^2]\} \leq 1 \qquad (1)$$

In terms of principle stresses, Eq. 1 can be rewritten as:

$$(\frac{1}{\sigma_t} - \frac{1}{\sigma_c})(\sigma_1 + \sigma 2 + \sigma 3) + \frac{1}{\sigma_t \sigma_c}\{\frac{1}{2}[(\sigma_1 - \sigma_2)^2 + (\sigma_2 - \sigma_3)^2 + (\sigma_3 - \sigma_1)^2]\} \leq 1. \qquad (2)$$

Alumina's tensile yield stress is one tenth of its compressive yield stress, so it is a brittle material. This imposes an additional failure criterion, that the maximum principle stress must be less than the tensile yield stress:

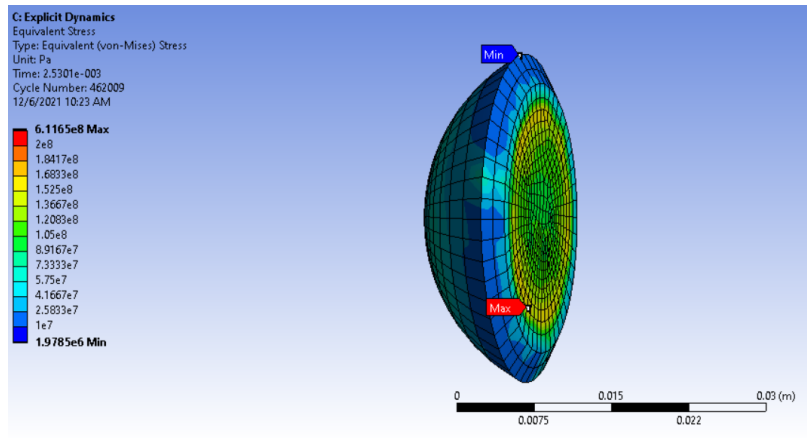$$Max(\sigma_1, \sigma_2, \sigma_3) \leq \sigma_t \qquad (3)$$

9

Fig. 16   Stress in Fully Dense Alumina Projectile Tip
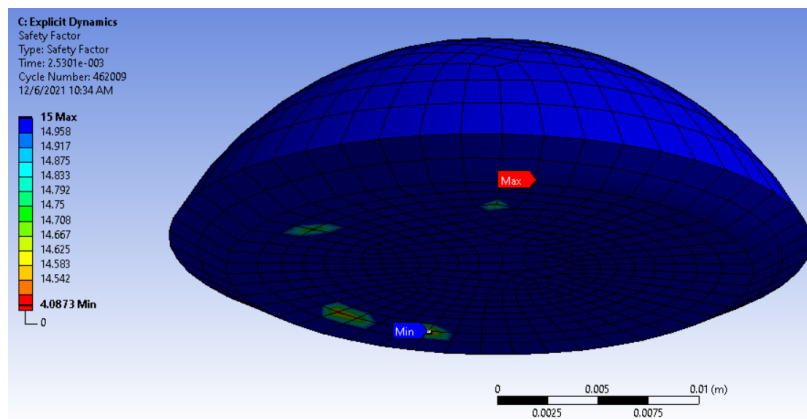

Fig. 17   Safety Factor in Fully Dense Alumina Projectile Tip
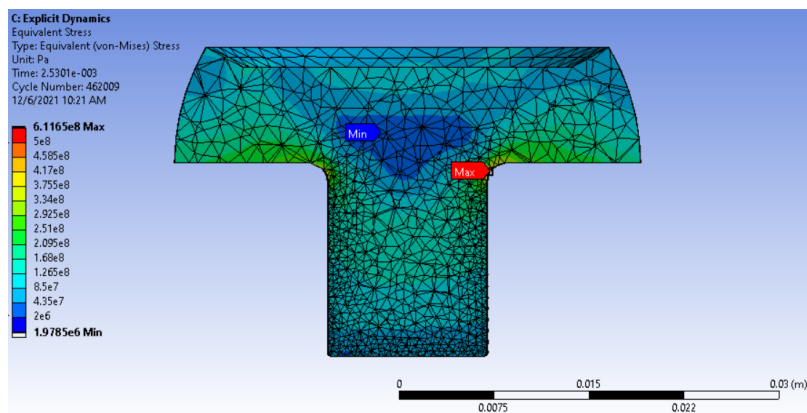

Fig. 18   Stress in Tungsten-Copper Projectile Tip Holder

Solving Eq. 2 with the simulated values for principle stress, it is found that the left side of the equation adds up to 0.57, which is safely less than 1. Eq. 3 is satisfied as well, since the maximum principle stress in the alumina tip is only 85 MPa, which is approximately three times less than the tensile yield stress of alumina.

Based on the successful execution of explicit dynamics simulations of an accelerating projectile, it was concluded that mechanical failure of the projectile during launch will be unlikely. High confidence was achieved that the full-bore-rider,
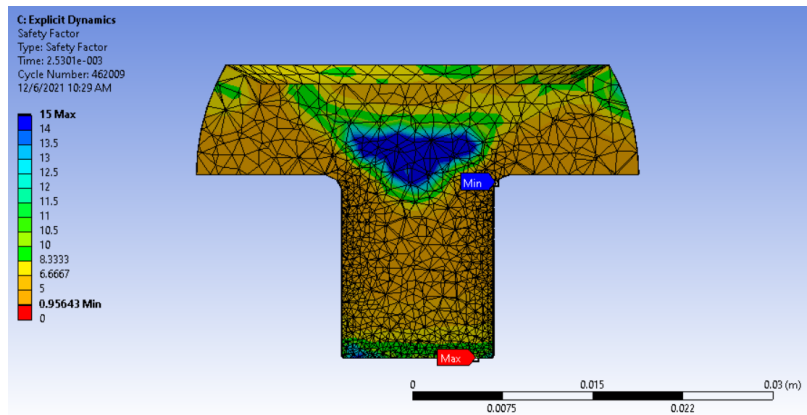
Fig. 19   Safety Factor in Tungsten-Copper Projectile Tip Holder

spherical-tipped projectile will avoid the sabot separation and stress wave concentration issues that troubled the earlier, slender projectiles. Parts were ordered and fabricated immediately thereafter. An assembled projectile prototype is depicted in Fig. 20
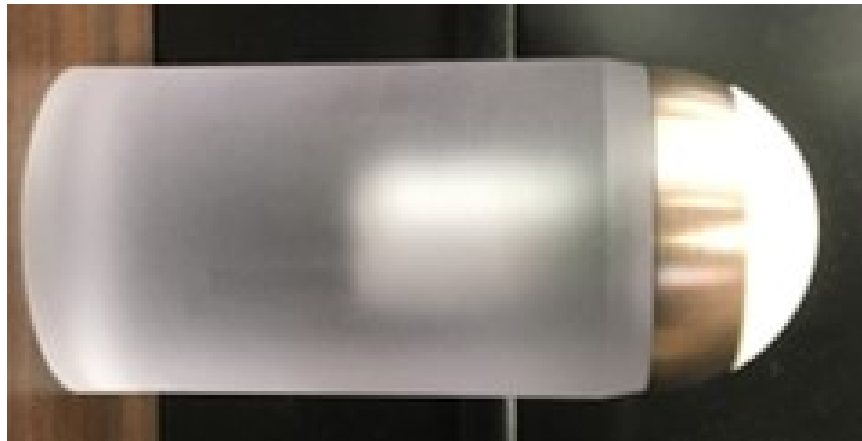

Fig. 20   Photograph of Assembled Full Bore Rider Projectile

VII. Future Testing

In the first quarter of 2022, test shots will be carried out with the modified full bore rider projectile design at a muzzle velocity of 2500 m/s. If these tests do not result in projectile breakup, blunt-tipped full bore rider projectiles can be used to study the interaction of multiphase flow fields with normal and detached shock structures. The slender projectiles made from 625 Inconel survived launch intact, and can be used to study multiphase flow interactions with oblique shock waves at high Mach numbers.

Tests at SwRI in 2022 will also incorporate devices built to manufacture liquid droplets of consistent size and spacing, and improved diagnostics hardware and techniques. Experiments with superior Schlieren imaging setups, planar laser-induced fluorescence (PLIF), and digital inline holography (DIH) will be performed at SwRI's LGG facility in preparation for in-depth studies of droplet breakup near projectiles at high Mach numbers.

VIII. Conclusion

Slender projectiles made from three different aerospace materials of interest were designed and fabricated for testing at SwRI's Light Gas Gun facility. The projectiles were mated to a sabot and accelerated to 2500 m/s. Of four shots attempted, only one proceeded without severe damage to the projectile. That shot used a projectile made of 625 Inconel.

11

Another test using 625 Inconel resulted in damage because of incomplete sabot separation. Tests using projectiles made from fully-dense alumina and carbon-carbon resulted in total projectile breakup before sabot separation. These shots revealed that high Mach number oblique shock interactions with multiphase flows can be studied with Inconel projectiles, but that a redesign is required to study multiphase flow interaction with more brittle aerospace materials. This redesign was performed and a finite element analysis simulation was conducted to increase confidence that the redesigned, blunt-tipped, full-bore-rider projectiles could survive the stress of launch in a gas gun. These results will be validated in early 2022 in a series of test shots at SwRI's LGG facility.

Acknowledgments

References

[1] Moylan, B., Landrum, B., and Russell, G., "Investigation of the Physical Phenomena Associated with Rain Impacts on Supersonic and Hypersonic Flight Vehicles," *Procedia Engineering*, Vol. 58, 2013, pp. 223–231. doi: 10.1016/j.proeng.2013.05.026.

[2] Lapp, R. R., Stutzman, R. H., and Wahl, N. E., "A Study of Rain Erosion in Plastics and Metals," WADC 53-185, 1954.

[3] Adler, W. F., "Investigation of Liquid Drop Impacts on Ceramics," ETI-CR-82-1075, 1982.

[4] Adler, W. F., "Rain impact retrospective and vision for the future," *Wear*, Vol. 233-235, 1999, pp. 25–38.

[5] Reinecke, W. G., and McKay, W. L., "Experiments on Water Drop Breakup Behind Mach 3 to 12 Shocks," SC-CR-70-6063, 1969.

[6] Barber, J. P., Taylor, H. R., Grood, E. S., and Hopkins, A. K., "Water Drop/Bow Shock Interactions," AFML-TR-75-105, 1975.

[7] Barber, J. P., "Water Drop Breakup/Impact Damage Thresholds," AFML-TR-76-126, 1976.

[8] Danehy, P. M., Weisberger, J., Johansen, C., Reese, D., Fahringer, T., Parziale, N. J., Dedic, C., Estevadeordal, J., and Cruden, B. A., "Non-Intrusive Measurement Techniques for Flow Characterization of Hypersonic Wind Tunnels," *Flow Characterization and Modeling of Hypersonic Wind Tunnels (NATO Science and Technology Organization Lecture Series STO-AVT 325)*, NF1676L-31725 - Von Karman Institute, Brussels, Belgium, 2018.

[9] Dworzanczyk, A., and Parziale, N. J., "High-Speed, Short-Pulse-Duration Light Source for Digital Inline Holographic Imaging of Multiphase Flow Fields," *Proceedings of AIAA Aviation Forum 2021*, AIAA-2021-2919, Virtual Event, 2021. doi: 10.2514/6.2021-2919.

[10] Mueschke, N. J., Walker, J. D., and Grosch, D., "Examination of Atmospheric Density Scaling Effects on Sub-Scale Hypersonic Flight Bodies Using a Ballistic Launch Facility," *Proceedings of the 23rd AIAA International Space Planes and Hypersonic Systems and Technologies Conference*, AIAA-2020-2444, Montreal, Quebec, Canada, 2020. doi: 10.2514/6.2020-2444.

[11] McMaster, "High-Strength 625 Nickel Rod, 1-Inch Diameter," , 2021. https://www.mcmaster.com/8791K115/,accessed 2021-6-01.

[12] SpecialMetals, "Inconel Alloy 625," , 2021. https://www.specialmetals.com/assets/smc/documents/alloys/inconel/inconel-alloy-625.pdf,accessed 2021-1-27.

[13] PrecisionCeramics, "Alumina (Aluminum Oxide)," , 2021. https://precision-ceramics.com/wp-content/uploads/2021/05/PC-USA-CeramAlox-202105.pdf,accessed 2021-6-01.

[14] Guelzo, D., "Carbon/Carbon Grade A200," , 2000. E-Mail, Received 2020-10-12.

[15] Bogdanoff, D. W., and Wilder, M. C., "Techniques for Transition and Surface Temperature Measurements on Projectiles at Hypersonic Velocities–A Status Report," Tech. rep., NASA Ames Research Center, 2005. NASA TM-2005-212831,.

[16] SchweissTechnik, "Wirbalit KW Tungsten Copper," , 2021. https://svs-schweisstechnik.de/files/downloads/tungsten_copper.pdf,accessed 2021-12-07.

[17] Mitsubishi, "PC 1000 Extruded, Unfilled, Polycarbonate (ASTM Product Data Sheet)," , 2020. `https://www.polymershapes.com/wp-content/uploads/2020/04/Polymershapes_MitsubishiChemicalAdvancedMaterials_DataSheet-PC-1000.pdf`,accessed 2021-12-07.

[18] Christensen, R. M., "A Comprehensive Theory of Yielding and Failure for Isotropic Materials," *J. Eng. Mater. Technol.*, Vol. 129(2), 2007, pp. 173–181. doi: 10.1115/1.2712847.